Inorganic Chemistry
Article

Inorg. Chem. **2009**, *48*, 11209–11214 **11209**
DOI: 10.1021/ic9016867

$Fe_5O_5[B_6O_{10}(OH)_3]\cdot nH_2O$: Wave-Layered Iron Borate and Frustrated Antiferromagnetism

Tao Yang,[†] Junliang Sun,[‡] Guobao Li,[†] Yingxia Wang,[†] Jeppe Christensen,[‡] Zhanbing He,[‡] Kirsten E. Christensen,[‡] Xiaodong Zou,[‡] Fuhui Liao,[†] and Jianhua Lin*[,†]

[†]*Beijing National Laboratory for Molecular Sciences, State Key Laboratory of Rare Earth Materials Chemistry and Applications, College of Chemistry and Molecular Engineering, Peking University, Beijing 100871, P.R. China, and* [‡]*Structural Chemistry, Stockholm University, SE-10691 Stockholm, Sweden*

Received August 25, 2009

The first layered iron borate, $Fe_5O_5[B_6O_{10}(OH)_3]\cdot nH_2O$, has been prepared by the boric acid flux method. Its structure, determined by single crystal X-ray diffraction, contains a double FeO_6-octahedral layer and an unusual $[B_6O_{13}]$ chain. The rigid and cambered $[B_6O_{13}]$ chains bend the octahedral layers, resulting in a wave-like and sandwiched structure. Crystallographic study indicates the structural modulation is mainly from the $[B_6O_{13}]$ chains because of the insertion of water molecules in between. Nevertheless, FeO_6 layers in the average structure, which are well separated by borate chains, is still a reasonable model to understand the two-dimensional magnetism. The strong antiferromagnetic interactions and the complex Fe^{3+}-net suggest a possible geometrically magnetic frustration, which may be the reason for the second-order temperature-induced magnetic transition at ~125 K. The condensed Fe^{3+} layers and the relatively low redox potential at about 1.25 V versus Li^+/Li show its potentials as an anodic material.

Introduction

Iron is an abundant and environmental-friendly transition metal element that exhibits various valence states from Fe^{2+} up to Fe^{6+}; hence, iron compounds attract particular attentions for their potential applications as electrochemical,[1] magnetic,[2] and catalytic[3] materials. Enormous efforts have been devoted to the structure−property relationship of iron-containing materials to understand the mechanism or to improve the performance in applications. A remarkable example was the long-lasting study on the "inductive effect" of different polyanions to the energy of Fe^{3+}/Fe^{2+} redox couple,[1] which led to the discovery of a promising cathode material of the olivine-type $LiFePO_4$ for lithium batteries.[1b] Because of the similarity in structures and properties, considerable attentions were also devoted to iron borates. In comparison with phosphates, however, there are only few iron borates known, that is, Fe_3BO_6, Fe_3BO_5, Fe_2BO_4, and $FeBO_3$.[4,5] All these compounds crystallize in 3D compact structures and lithium-intercalation always leads to collapse of the structure frameworks. Nevertheless, some iron borates did show unique magnetic properties, such as transparent magnetic property of $FeBO_3$, which may have potential in visible magneto-optical devices.[2c] To explore new borate phases, we carried out a systematic study on syntheses in boric acid flux.[6] Here we report a new iron hydroxyborate, $Fe_5O_5[B_6O_{10}(OH)_3]\cdot nH_2O$ (**1**). **1** is the first layered iron borate consisting of double FeO_6 octahedral layers and $[B_6O_{13}]$ triangular chains. The $[B_6O_{13}]$ is a rigid cambered chain that bends the double FeO_6 octahedral layer forming a fascinating wave-like 2D structure.

*To whom correspondence should be addressed. E-mail: jhlin@pku.edu.cn. Phone: (8610)62751715. Fax: (8610)62751708.

(1) (a) Masquelier, C.; Padhi, A. K.; Nanjundaswamy, K. S.; Goodenough, J. B. *J. Solid State Chem.* **1998**, *135*, 228. (b) Padhi, A. K.; , Nanjundaswamy, K. S.; , Goodenough, J. B. *Proceedings of the 189th ECS Meeting*, Los Angeles, CA, May 1996.

(2) (a) Einaga, Y.; Taguchi, M.; Li, G. M.; Akitsu, T.; Gu, Z. Z.; Sugai, T.; Sato, O. *Chem. Mater.* **2003**, *15*, 8. (b) Kimel, A. V.; Pisarev, R. V.; Hohlfeld, J.; Rasing, T. *Phys. Rev. Lett.* **2002**, *89*, 287401. (c) Shang, S. L.; Wang, Y.; Liu, Z. K.; Yang, C. E.; Yin, S. Z. *App. Phys. Lett.* **2007**, *91*, 253115.

(3) (a) Kim, J.; Nielsen, U. G.; Grey, C. P. *J. Am. Chem. Soc.* **2008**, *130*, 1285. (b) Yuan, Z. Y.; Ren, T. Z.; Su, B. L. *Catal. Today* **2004**, *93*−*95*, 743–750.

(4) (a) Ibarra-Palos, A.; Darie, C.; Proux, O.; Hazemann, J. L.; Aldon, L.; Jumas, J. C.; Morcrette, M.; Strobel, P. *Chem. Mater.* **2002**, *14*, 1166. (b) Diehl, R. *Solid State Commun.* **1974**, *17*, 743. (c) Diehl, R.; Brandt, G. *Acta Crystallogr., Sect. B* **1975**, *31*, 1662. (d) Attfield, J. P.; Clarke, J. F.; Perkins, D. A. *Physica B* **1992**, *180*, 581. (e) Swinnea, J. S.; Steinfink, H. *Am. Mineral.* **1983**, *68*, 827.

(5) (a) Legagneur, V.; An, Y.; Mosbah, A.; Portal, R.; Le Gal La Salle, A.; Verbaere, A.; Guyomard, D.; Piffard, Y. *Solid State Ionics* **2001**, *139*, 37. (b) Dong, Y. Z.; Zhao, Y. M.; Shi, Z. D.; An, X. N.; Fu, P.; Chen, L. *Electrochim. Acta* **2008**, *53*, 2339.

(6) (a) Ju, J.; Lin, J. H.; Li, G. B.; Yang, T.; Li, H. M.; Liao, F. H.; Loong, C.-K.; You, L. P. *Angew. Chem., Int. Ed.* **2003**, *42*, 5607. *Angew. Chem.*, **2003**, *115*, 5765;(b) Lin, J. H.; Sheptyakov, D.; Wang, Y. X.; Allenspach, P. *Chem. Mater.* **2004**, *16*, 2418. (c) Yang, T.; Ju, J.; Li, G. B.; Liao, F. H.; Zou, X. D.; Deng, F.; Chen, L.; Wang, Y. X.; Lin, J. H. *Inorg. Chem.* **2007**, *46*, 4772. (d) Ju, J.; Lin, J. H.; Yang, T.; Li, G. B.; Liao, F. H.; Wang, Y. X.; You, L. P. *Chem. J. Eur.* **2004**, *10*, 3901.

© 2009 American Chemical Society
Published on Web 10/26/2009

Experimental Section

All reagents are of analytical grade and were used as obtained from commercial sources without further purification. A typical synthesis was to charge $FeCl_3 \cdot 6H_2O$ (2 mmol), H_3BO_3 (50 mmol), and 1−3 drops of concentrated hydrochloric acid (36%∼38%) into a 50 mL unsealed Teflon container, which was then sealed in a steel autoclave and further heated at 240 °C for 5 days. After cooling down to the room temperature, the solid product was extensively washed by distilled water, and the yield was about 75%.

Single crystal X-ray diffraction data of **1** (0.18 × 0.08 × 0.04 mm^3) were collected at 100 K on an Xcalibur3 diffractometer equipped with a CCD camera using Mo Kα radiation (λ = 0.71073 Å) from an enhanced optic X-ray tube. Data integration and numerical absorption correction were carried out with the Crysalis software package from Oxford Diffraction. With the average unit cell ($P2/c$, a = 3.8197(2), b = 11.8571(5), c = 16.2617(8) Å, β = 103.620(5)°), a total of 9728 reflections, of which 1448 were unique (R_{int} = 0.0238), were collected in the region 3.67° < θ < 36.51°. The structure solution and refinement were carried out using the SHELX-97 software package[7] with R_1 = 0.0413 and wR_2 = 0.1084 for all reflections. The data set of the 4-fold superstructure ($P2/c$, a = 15.3013(4), b = 11.8762(4), c = 16.2894(5) Å, β = 103.627(2)°) was extracted from the same data collection (36235 reflections with 5068 unique) with R_{int} = 0.0375. The refinement was converged with R_1 = 0.0569 and wR_2 = 0.1765. Because of serious twinning and disorder, only Fe atoms were refined with anisotropic thermal parameters. Further details on the crystal structure investigations may be obtained from the Fachinformationszentrum Karlsruhe, 76344 Eggenstein-Leopoldshafen, Germany (fax: (+49)7247−808−666; e-mail: crysdata@fiz-karlsruhe.de), on quoting the depository number CSD-418739.

Selected area electron diffraction (SAED) was performed on a JEOL JEM-3010 at 300 kV with a Gatan Multiscan 600HP CCD camera. Single crystals of **1** were first ground slightly, dispersed in ethanol by ultrasound, and then a drop of the suspension was transferred onto a copper grid covered by holey carbon films. Crystals with sharp angles and edges were selected for the electron microscopy studies, and they are about a few μms with irregular shapes. The regions about a few hundred nms around the tips of the sharp angles were selected for the SAED. The magnetic susceptibility was carried out on a Quantum Design MPMS XL-7 SQUID from T = 2 to 350 K under an applied field of 100 Oe. The Mössbauer spectra of **1** were recorded with a constant acceleration spectrometer equipped with a rhodium matrix cobalt-57 source that had been calibrated at room temperature with α-iron foil. FT-IR spectroscopy was measured with a Nicolet Magna-IR-750 series II. Thermogravimetric (TG) analysis was carried out on a Dupont 951 Thermogravimetric Analyzer in air with a heating rate of 10 °C/min from 40 to 750 °C.

Results and Discussions

Structure. The as-obtained $Fe_5O_5[B_6O_{10}(OH)_3] \cdot nH_2O$ from the flux of boric acid are golden-brown and lamellar-shaped single crystals (Figure 1). Both electron and single X-ray diffraction studies indicate 4-fold or 5-fold monoclinic super-reflections (a = 15.3 or 19.1 Å, b = 11.9 Å, c = 16.3 Å, β = 103.6°), which depend on individual crystals, superimposed on a pseudo-orthorhombic unit cell. However, because of the weak intensities of super reflections,

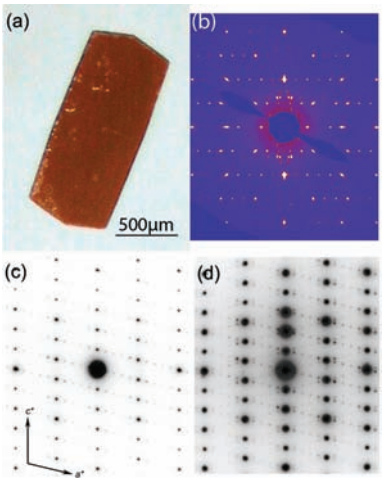

Figure 1. (a) Morphology of the as-synthesized $Fe_5O_5[B_6O_{10}(OH)_3] \cdot nH_2O$ single crystal; (b) single crystal diffraction frame shows 4-fold super lattice and twinning problem of the selected crystal; (c) ED pattern shows 5-fold super lattice; (d) ED pattern shows twinning problem.

Table 1. Atomic Coordinates and Isotropic Displacement Parameters (Å^2) in the Average Structure Model

atom	Wyckoff position	x	y	z	U_{eq}	BVS
Fe1	4 g	0.11809(16)	0.37445(5)	0.36806(4)	0.0085(2)	2.950
Fe2	4 g	0.30960(16)	0.44447(6)	0.55955(4)	0.0095(2)	3.167
Fe3	2f	0.5000	0.49193(8)	0.7500	0.0078(2)	2.864
B1	4 g	0.124(3)	0.1182(6)	0.3740(5)	0.044(2)	3.131
B2	4 g	0.265(3)	0.2027(6)	0.5150(5)	0.057(3)	3.095
B3	4 g	0.425(3)	0.2473(7)	0.6725(4)	0.045(2)	3.058
O1	2e	0.0000	0.5443(4)	0.7500	0.0090(9)	1.816
O2	4 g	−0.1935(8)	0.4818(3)	0.55684(19)	0.0096(6)	2.055
O3	4 g	0.6089(8)	0.4143(3)	0.35896(19)	0.0095(6)	1.962
O4	4 g	0.4171(9)	0.3610(3)	0.6662(2)	0.0160(7)	2.109
O5	4 g	0.2370(9)	0.3085(3)	0.4877(2)	0.0162(7)	2.148
O6	4 g	0.0786(10)	0.2157(3)	0.3287(2)	0.0181(7)	1.579
O7	4 g	0.085(3)	0.0183(5)	0.3345(4)	0.119(4)	1.090
O8	4 g	0.210(2)	0.1146(4)	0.4605(3)	0.080(3)	2.055
O9	2f	0.5000	0.1951(5)	0.7500	0.048(2)	1.994
O10	4 g	0.351(4)	0.1802(5)	0.6021(4)	0.167(6)	1.928

the structure was first determined in a monoclinic subcell, $P2/c$, a = 3.8197(2) Å, b = 11.8571(5) Å, c = 16.2617(8) Å, β = 103.620(5)°. The average structure consists of 16 unique non-hydrogen atoms, that is, 3 Fe, 3 B, and 10 O. Among them, Fe3, O1, and O9 are located on a 2-fold axis, and the rest are all in general positions. The atomic coordinates, anisotropic displacement parameters, selected bond distances and angles are given Tables 1−4. All are in reasonable ranges for typical Fe−O and B−O bonds.

All Fe atoms are octahedrally coordinated in **1**, forming a layer perpendicular to the b-axis as shown in Figure 2a. In fact, the FeO_6 octahedral layer can be considered as a derivative of the γ-FeOOH layer[8] or, in other words, a derivative of double rock salt layer in the [110] direction (Figure 2b), which features in extensive edge-sharing and zigzag-like buckled triangular Fe-net (Figure 2c). Although the FeO_6 octahedral layer in **1** is bent, the fundamental Fe-nets are quite similar, except

(7) Sheldrick, G. M., *SHELXS 97, Program for the solution of crystal structures*; University of Göttingen: Göttingen, Germany, 1997. *SHELXL 97, Program for the refinement of crystal structures*; University of Göttingen: Göttingen, Germany, 1997.

(8) Christensen, H.; Christensen, A. N. *Acta Chem. Scand. A* **1978**, *32*, 87.

Table 2. Anisotropic Displacement Parameters (Å^2) in the Average Structure Model

atom	U_{11}	U_{22}	U_{33}	U_{23}	U_{13}	U_{12}
Fe1	0.0066(3)	0.0119(4)	0.0077(4)	0.0000(2)	0.0027(2)	0.0000(2)
Fe2	0.0062(3)	0.0157(4)	0.0071(4)	−0.0009(2)	0.0025(2)	−0.0003(2)
Fe3	0.0065(4)	0.0109(5)	0.0066(4)	0.000	0.0025(3)	0.000
B1	0.088(7)	0.022(4)	0.017(3)	−0.001(3)	0.005(4)	−0.001(4)
B2	0.132(9)	0.014(3)	0.018(3)	0.000(3)	0.008(4)	−0.003(4)
B3	0.092(7)	0.025(4)	0.015(3)	0.002(3)	0.007(4)	0.002(4)
O1	0.009(2)	0.011(2)	0.007(2)	0.000	0.0019(16)	0.000
O2	0.0074(14)	0.0134(16)	0.0085(15)	−0.0015(12)	0.0028(11)	−0.0004(12)
O3	0.0065(14)	0.0137(16)	0.0090(14)	0.0008(12)	0.0035(11)	0.0002(12)
O4	0.0255(19)	0.0121(16)	0.0102(16)	−0.0009(13)	0.0038(14)	−0.0006(14)
O5	0.0241(18)	0.0141(16)	0.0104(15)	0.0004(13)	0.0042(13)	−0.0004(14)
O6	0.0276(19)	0.0109(17)	0.0151(17)	−0.0025(13)	0.0036(14)	−0.0004(14)
O7	0.291(13)	0.017(3)	0.035(3)	−0.003(2)	0.011(5)	−0.001(5)
O8	0.194(8)	0.016(2)	0.023(3)	0.002(2)	0.010(4)	0.001(3)
O9	0.111(6)	0.010(3)	0.020(3)	0.000	0.008(3)	0.000
O10	0.445(19)	0.016(3)	0.021(3)	0.002(2)	0.017(6)	−0.002(6)

Table 3. Selected Bond Distances in the Average Structure Model

bond	distance (Å)	bond	distance (Å)	bond	distance (Å)
Fe1−O3	1.972(3)	Fe2−O2	1.962(3)	B1−O7	1.339(9)
Fe1−O3	1.973(3)	Fe2−O5	1.972(3)	B1−O6	1.359(8)
Fe1−O6	1.983(3)	Fe2−O2	2.037(3)	B2−O5	1.327(8)
Fe1−O5	2.046(3)	Fe2−O3	2.113(3)	B2−O8	1.354(9)
Fe1−O2	2.077(3)	Fe3−O1 × 2	2.0083(14)	B2−O10	1.402(10)
Fe1−O1	2.100(2)	Fe3−O4 × 2	2.041(3)	B3−O4	1.352(9)
Fe2−O4	1.955(3)	Fe3−O3 × 2	2.050(3)	B3−O10	1.368(9)
Fe2−O2	1.959(3)	B1−O8	1.368(9)	B3−O9	1.372(8)

Table 4. Selected Bond Angles in the Average Structure Model

angle	amplitude (deg)	angle	amplitude (deg)	angle	amplitude (deg)
O3−Fe1−O6	101.79(14)	O4−Fe2−O2	97.59(14)	O1−Fe3−O4	103.49(13)
O3−Fe1−O6	101.79(14)	O4−Fe2−O2	97.71(14)	O1−Fe3−O4	103.73(14)
O3−Fe1−O5	99.24(14)	O4−Fe2−O5	94.74(14)	O1−Fe3−O4	103.73(13)
O3−Fe1−O5	99.04(14)	O2−Fe2−O5	99.96(14)	O1−Fe3−O4	103.49(14)
O6−Fe1−O5	85.82(14)	O2−Fe2−O5	99.83(14)	O4−Fe3−O4	80.94(19)
O3−Fe1−O2	81.09(13)	O2−Fe2−O2	83.24(13)	O1−Fe3−O3	80.37(10)
O3−Fe1−O2	81.12(13)	O2−Fe2−O2	83.37(13)	O1−Fe3−O3	80.31(10)
O5−Fe1−O2	77.62(13)	O5−Fe2−O2	80.26(14)	O4−Fe3−O3	82.39(13)
O3−Fe1−O1	79.92(9)	O4−Fe2−O3	82.87(13)	O1−Fe3−O3	80.31(10)
O3−Fe1−O1	79.97(9)	O2−Fe2−O3	80.49(12)	O1−Fe3−O3	80.37(10)
O6−Fe1−O1	99.02(15)	O2−Fe2−O3	80.46(12)	O4−Fe3−O3	82.39(13)
O2−Fe1−O1	97.54(14)	O2−Fe2−O3	102.13(13)	O3−Fe3−O3	114.28(18)
O8−B1−O7	116.0(6)	O5−B2−O8	121.5(6)	O4−B3−O10	121.3(6)
O8−B1−O6	123.6(6)	O5−B2−O10	120.0(6)	O4−B3−O9	121.0(6)
O7−B1−O6	120.4(6)	O8−B2−O10	118.5(6)	O10−B3−O9	117.6(7)

that few Fe-triangles are interrupted by the presence of corner-sharing connections as shown in Figure 2d.

The boron atoms in the structure are all triangularly coordinated, which share corners forming a $[B_6O_{13}]$ polyborate anion. The $[B_6O_{13}]$ groups further share corners with the Fe-octahedral layer forming a sandwich-like layered structure (Figure 3). $[B_6O_{13}]$ is a very unusual borate chain. It consists of merely BO_3 and, furthermore, all BO_3 groups are oriented in the same direction. $[B_6O_{13}]$ is rigid, represented by its characteristic mean O−B−O angle of 120° and B−O−B angle of 129°. The cambered $[B_6O_{13}]$ chain could also be considered as part of a circumference. Further expanding the borate chain, one would get a large and symmetric circular borate anion with 40 boron atoms $[B_{40}O_{80}]^{40-}$. Although such a large circular borate anion may not be realistic, the presence of the cambered $[B_6O_{13}]$ chain is remarkable, which bends the double octahedral layer, interrupts the edge-sharing, and introduces the corner-sharing in every six FeO_6 octahedra, and finally leads to an unusual wave-like layered structure.

Carefully examining the average structure reveals abnormally elongated thermal ellipsoids along the *a*-axis for the oxygen atoms of borate groups, especially for O7 and O10 (see Table 2 and Figure 4), implying that the modulation arises mainly from borate groups. The O7 is a terminal oxygen of the $[B_6O_{13}]$ group; thus having a large displacement parameter is not uncommon. However, a large displacement is unusual for the bridging oxygen O10. We, therefore, expanded the average structure into a 4-fold supercell, while maintaining the structure framework. Iron atoms in the superstructure were refined anisotropically, while others (B and O) are described with isotropic displacement parameters because of the weak

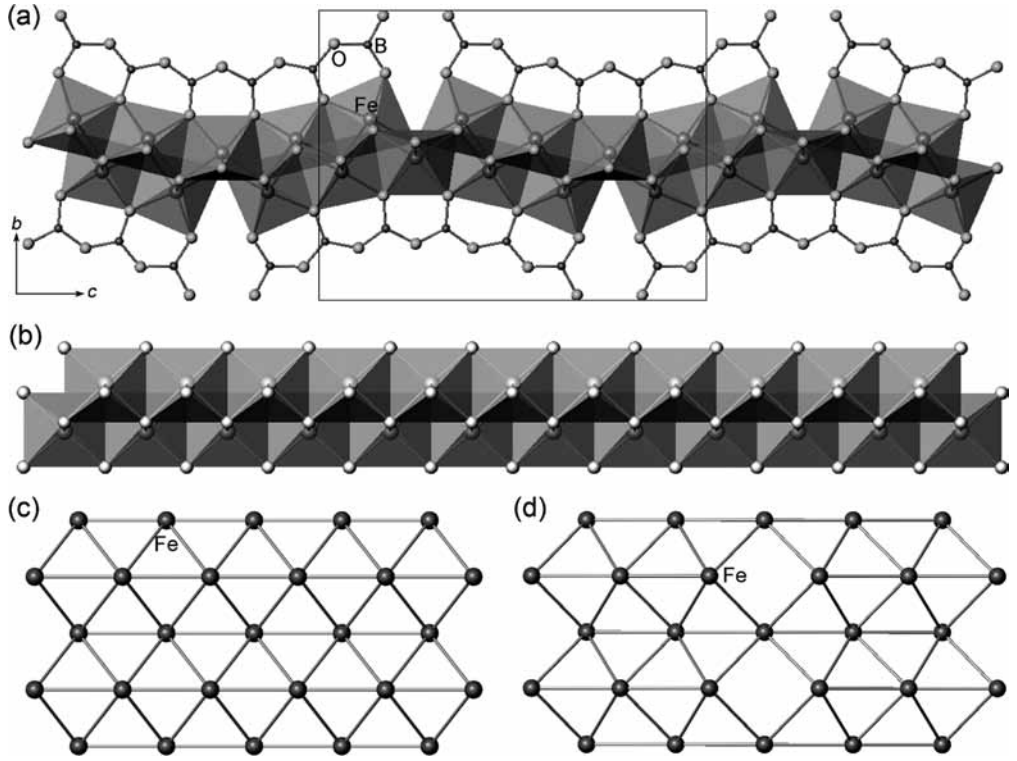

Figure 2. Comparison of the layers in **1** and lepidocrocite FeOOH; (a) the wave-like layer in **1** viewing along the *a*-axis showing Fe-octahedra and borate chains; (b) octahedral layer in FeOOH; (c) and (d) the Fe-net in FeOOH and **1**.

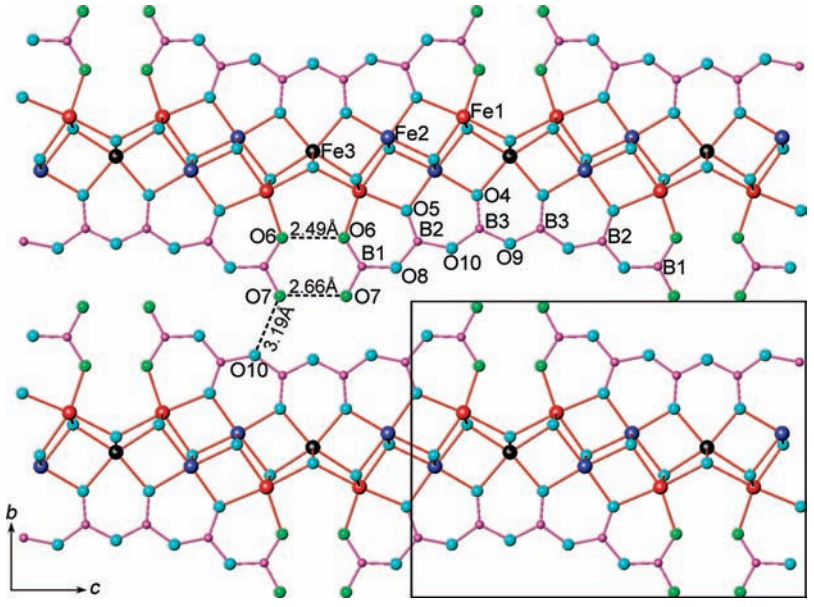

Figure 3. Structural view of **1** along *a*-axis emphasizing the local coordination environments of iron and boron atoms and, possible hydrogen bonds. Black, red, and deep blue spheres represent crystallographically independent Fe atoms. B and O are presented as purple and sky blue spheres, respectively. O bonded to H are highlighted as green spheres.

super-reflections and strong correlations. This 4-fold superstructure model provides further insights for the origin of modulation and the unusual thermal ellipsoids in the average structure: first, additional water molecules were identified in an ordered fashion between every two $[B_6O_{13}]$ chains (Figure 5). The inserted water molecules induce the 4-fold superstructure and, additionally, they push the neighboring $[B_6O_{13}]$ chains off the ideal positions, which lead to relatively large displacement parameters for the O8, O9, and O10 in the average structure. Second, according to the O−O distances, there are considerable numbers of hydrogen bonds within and between the layers. The large displacement parameter of O7 originates mainly from the hydrogen bond to the O10 in the neighboring layer and the insert H_2O (Figure 3 and in the Supporting Information, Figure S1). Nevertheless, it is clear that the insert water molecule modifies the structure but does not change the structure framework

(especially the Fe-framework); thus, the average structure is still a reasonable model with which to understand the structure of this layered iron hydoxyborate.

According to the structure determination, the non-hydrogen composition of **1** is $[Fe_5B_6O_{18}]$. To obtain the complete composition, one needs to address the oxidation state of Fe ions and the possible protons in the structure. The ^{57}Fe Mössbauer spectrum (Figure 6) shows that, in the first place, the iron atoms in **1** are all high-spin Fe^{3+}. Additionally two different Fe ions in a ratio of 2:3 were identified in the spectrum. We knew that all FeO_6 octahedra in the structure are surrounded by eight neighboring octahedra, but their connections are different. Fe2 and Fe3 have six edge-sharing and two corner-sharing neighbor octahedra; while for Fe1, there are five edge-sharing and three corner-sharing (see Supporting Information, Figure S2). The ratio of these two kinds of iron atoms (Fe1:(Fe2+Fe3)) is 2:3, which agrees with that found in the Mössbauer spectrum.

The bond valence sums (BVS) calculation shows that most of the atoms are normal except O6 and O7 (O6, 1.579 and O7, 1.090, see Table 1), indicating the presence of protons around these positions. TG measurement, on the other hand, shows three distinct steps of weight-loss (see Figure 7a). The first weight-loss (1.06 wt %) at about 300 °C originates from the removal of the adsorbed water (calcd 1.39 wt %, based on $Fe_5O_5[B_6O_{10}(OH)_3]\cdot 0.5H_2O$ from the single crystal X-ray diffraction study), while the other two at about 500 and 780 °C attribute to the dehydration of the hydroxyl group in the structure (exp. 4.18 wt %, calcd 4.19 wt %). The discrepancy of the portions of absorbed water from the structure solution and TG analysis is reasonable because the single crystals show diverse water absorptions, which might also be the reason there are both 4-fold and 5-fold superstructures. IR absorption bands around 3000−3500 cm^{-1} support the presence of hydroxyl groups and water molecules in the structure (see Figure 7b). Additionally, we carried out a preliminary cyclic voltammogram measurement (see Supporting Information, Figure S3), which shows a redox potential of about 1.25 V versus Li^+/Li, similar to that of $FeBO_3$.[4a]

Magnetism. According to the crystal structure of **1**, two-dimensional magnetism is expected because of the long interlayer distance (~10 Å) which prevents any reasonable magnetic interactions between the layers. The complex Fe-net (see Figure 2d) makes it impossible to simulate the magnetic susceptibility curve by applying simple models. Qualitative analyses are as follows: as shown in Figure 8, **1** has significantly small susceptibility (i.e., a low χT value ~1.34 $cm^3\cdot K\cdot mol^{-1}$ at 360 K, in comparison with the theoretical value of 4.375 $cm^3\cdot K\cdot mol^{-1}$ in the paramagnetic state), which indicates fairly strong antiferromagnetic (AFM) interactions

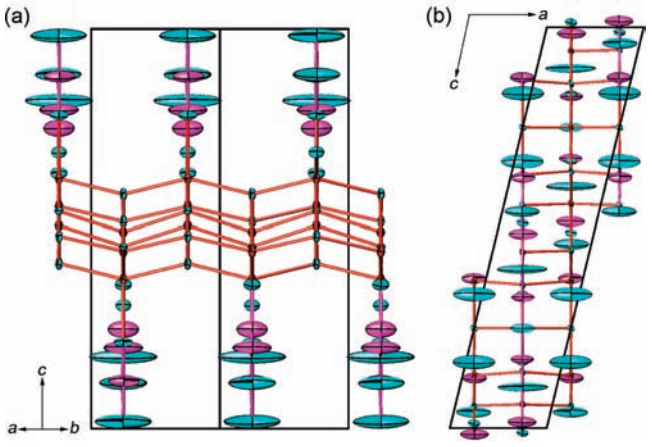

Figure 4. Structural views along the [101] and [010] directions of **1**. Red, purple, and sky blue are Fe, B, and O, respectively. Anisotropic displacement parameters for atoms are represented as ellipsoids.

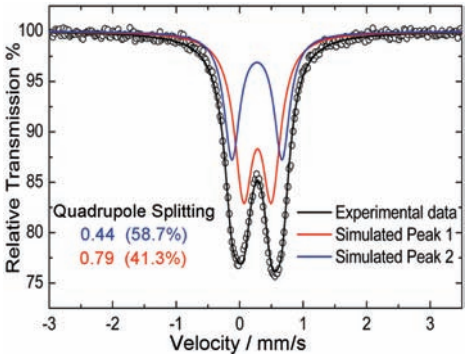

Figure 6. ^{57}Fe Mössbauer spectrum at room temperature; simulated and experimental curves are shown.

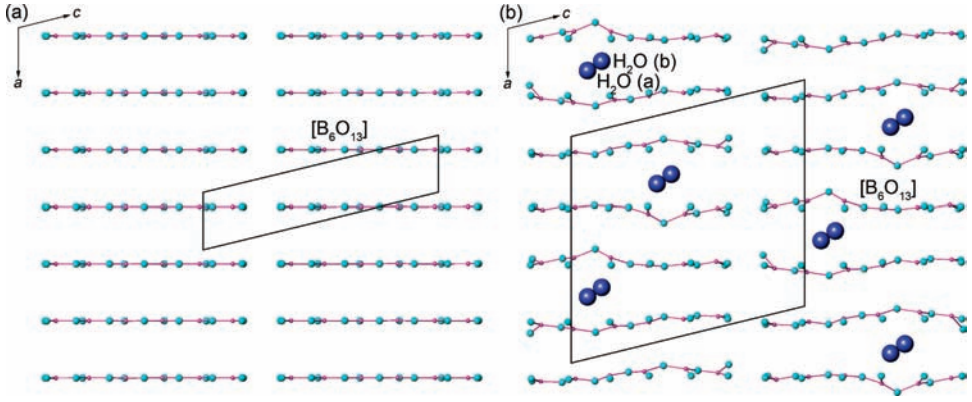

Figure 5. The arrangement of $[B_6O_{13}]$ chains in **1**. The left figure shows the parallel $[B_6O_{13}]$ chains in the average structure model; the right one shows the location of the insert water molecules in the 4-fold super structure model, where H_2O (a) and H_2O (b) are two partially occupied water molecules and their total occupancy is unit. Purple, sky blue and deep blue are B, O, and H_2O, respectively.

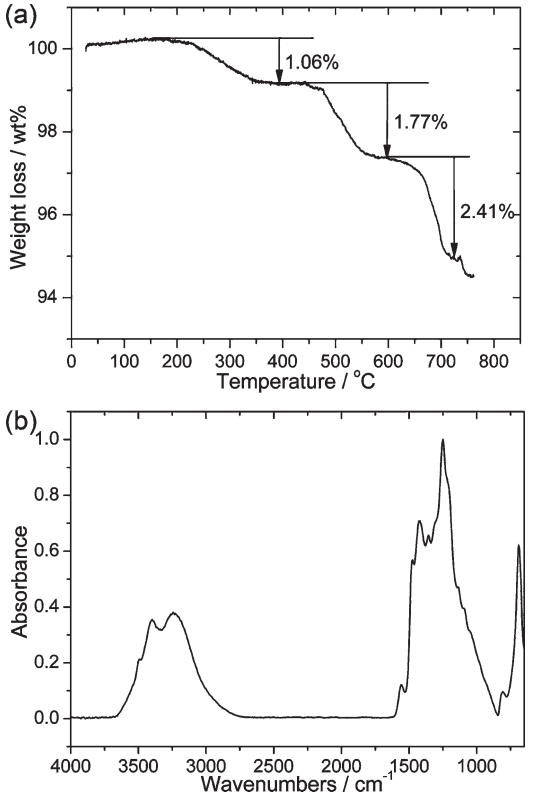

Figure 7. (a) TG curve and (b) FT-IR spectrum of **1**.

between Fe^{3+} cations; a broad maximum of χ at about 300 K (inset of Figure 8) is a typical sign of the onset of a short-range magnetic order for low-dimensional systems, which is consistent with the inability to fit the magnetic susceptibility data to the Curie−Weiss law.

The most significant feature of $\chi-T$ curve is the sharp increase at ~125 K for both ZFC and FC curves followed by a bifurcation. This peak retains at high external field (see Supporting Information, Figure S4). The alternating current (ac) susceptibility shows a broad peak at the same temperature (see Supporting Information, Figure S5), suggesting a second-order phase transition. The isothermal magnetizations measured at different temperatures (from 83 to 123 K) look quite similar, which exhibit almost a linear dependence on the external magnetic field up to 6 T with a small remanence below 120 K. Moreover, although the remanence is very small, it still exhibits a temperature-dependence behavior with a maximum coincidence with the ZFC susceptibility (Figure 8 and Supporting Information, Figure S6).

The possibility of a structural transition at ~125 K could be ruled out because the single X-ray diffraction study shows that the structure is the same at 100 K and at room temperature. Thus, a magnetic transition is responsible.

Usually, a bifurcation of the ZFC and FC curves points to a spontaneous ferromagnetic moment or spin glass. Since there is no sharp increase in the field-dependent magnetization curves, the glassy magnetism is the cause of the bifurcation of ZFC/FC as well as of the small

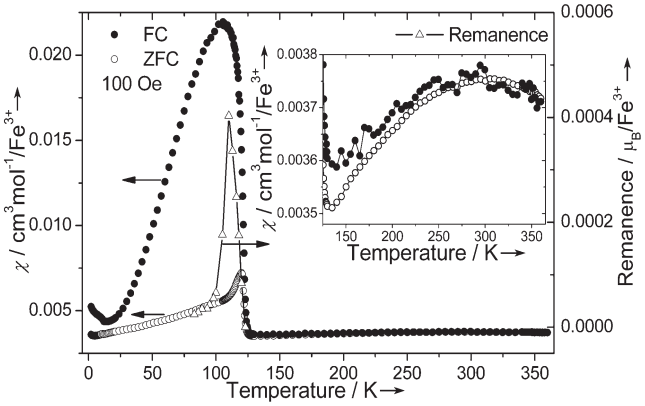

Figure 8. ZFC and FC dc susceptibility and variation of the remanence as a function of temperature for **1**; inset is an enlargement for high temperature data (125 K < T < 360 K).

remanence in isothermal magnetizations. According to the complex Fe-net and the strong AFM interactions in **1**, geometrically magnetic frustration is not surprising, and the well-known character of frustrated systems is, theoretically, the inability to an unique ground magnetic state. In **1**, we attribute the temperature-induced magnetic transition at ~125 K to be a second-order transition from one 2D magnetic order to the other one, and at the transition temperature range (83−125K), the competition between two magnetic phases leads to the glassy behavior. Further study is necessary to confirm this hypothesis. The rise of χ at lower temperature (~15 K) may originate from paramagnetic impurities in the sample.

Conclusion

As the first layered iron borate, the structure of $Fe_5O_5[B_6O_{10}(OH)_3]\cdot nH_2O$ (**1**) is a fascinating one that contains a double Fe-octahedral layer and an unusual $[B_6O_{13}]$ chain. The rigid and cambered $[B_6O_{13}]$ chains bend the octahedral layers, resulting in a wave-like and sandwiched structure. The interaction between the Fe^{3+} ions is antiferromagnetic. A possible temperature-induced magnetic transition happens with respect to the sharp anomaly at ~125 K in $\chi-T$. In addition, the condensed Fe^{3+} layers and relatively low redox potential at about 1.25 V versus Li^+/Li remind us of the potentials as an anodic material. However, more extensive electrochemical study is needed to fully understand what happened during the electrochemical process, and to improve the performance of the material.

Acknowledgment. This work was supported by the Nature Science Foundation of China; we are thankful to Prof. Zhou and W. Liu for their assistance with the electrochemical measurements.

Supporting Information Available: Crystal details in CIF formats, cyclic voltammogram, dc susceptibility at 20 kOe, ac susceptibilities and isothermal magnetizations. This material is available free of charge via the Internet at http://pubs.acs.org.